Journal of Photochemistry & Photobiology, A: Chemistry 456 (2024) 115805

Contents lists available at ScienceDirect

Journal of Photochemistry & Photobiology, A: Chemistry

journal homepage: www.elsevier.com/locate/jphotochem

Invited paper

Visible light active Ag@$SrTiO_3$: A powerful photocatalyst for NO_x degradation

Marcela Frias Ordoñez [a,b], Ermelinda Falletta [a,b,*], Giuseppina Cerrato [c], Claudia L. Bianchi [a,b]

[a] Department of Chemistry, Università degli Studi di Milano, Via C. Golgi 19, 20133 Milano, Italy
[b] Consorzio Interuniversitario Nazionale per la Scienza e Tecnologia dei Materiali (INSTM), Via Giusti 9, 50121 Florence, Italy
[c] Department of Chemistry, University of Turin, Via Pietro Giuria 7, 10125 Turin, Italy

ARTICLE INFO

Keywords:
NO_x abatement
Strontium titanate
Metal decoration
Photocatalysis
LED light

ABSTRACT

Exploiting visible light for NO_x degradation represents an important challenge to enhance the air quality of our environment. In the present study, the photocatalytic activities of two commercial strontium titanate (STO) having different sizes (micro and nano) were compared towards NO_x degradation under LED light. The decoration of both STO photocatalysts by Ag nanoparticles (8 theoretical wt.%) led to enhanced photocatalytic efficiency more than twice. In particular, nano-sized Ag@STO showed the highest activity (75% of NO_x degradation) within 180 min due to Ag nanoparticles (NPs) localized surface plasmon resonance (LSPR) properties and the large surface area of nano-STO. The photocatalysts were synthesized by the wet impregnation method and calcined at 400 °C. Their structural, morphological, specific surface area, and optical properties were characterized by X-ray diffraction (XRD), Field Emission Scanning Electron Microscopy (FESEM), N_2 adsorption/desorption analysis, and UV–Vis diffuse reflectance spectroscopy (DRS).

1. Introduction

Over the past decades, due to the fast growth of anthropogenic activities, nitrogen oxides (NO_x) emissions have risen considerably, and their abatement has become a scientific challenge and a global need [1]. The attempted strategies to successfully deal with this issue have led to the development of several advanced techniques, such as selective catalytic reduction (SCR) and selective non-catalytic reduction (SNCR) approaches, among others. In both these technologies NO_x are selectively reduced to N_2 by employing reducing agents such as NH_3 or urea. In SCR the presence of a catalyst benefits the reaction at lower temperatures (250–450 °C), whilst in SNCR, due to the absence of a catalyst, NO_x conversion takes place at temperatures higher than 850 °C (up to 1100 °C) [2,3]. Alternatively, photocatalysis represents an environmentally friendly and promising technology for the degradation of organic and inorganic pollutants at ambient conditions [3–5]. Titanium dioxide (TiO_2) is a remarkable photocatalyst that has been ubiquitously studied because of its low cost, abundance, and high photocatalytic efficiency under UV light [6]. However, its wide energy bandgap (~3.2 eV) restricts its light absorption to 5 % of the total solar spectrum [7]. There have been attempts directed toward overcoming this drawback. For instance, by properly modifying the TiO_2 lattice with transition metals, non-metal ions, or noble metals, its response under visible light irradiation can be easily enhanced [8]. Ma *et al.* [9,10] successfully prepared a 0.1 % Fe/TiO_2 catalyst by incorporating Fe into the TiO_2 lattice through the co-precipitation method. After 30 min of reaction, the photocatalytic performance toward NO_x was double that of bare TiO_2. Moreover, it exhibited the lowest NO_2 selectivity (31 %) and the highest conversion of NO_x (38 %) compared to other samples. The enhancement was ascribed to the incorporation of Fe^{3+} ions as electron-trapping agents, which facilitate electron-hole separation and improve TiO_2 photocatalytic activity under visible light irradiation. On the other hand, Patzsch *et al.* [9,11,12] employed in their study an impregnation method to graft commercially available TiO_2 (Aeroxide P25) with small amounts of iron ions. The authors observed that increasing the iron concentration in Fe-TiO_2 catalysts from 0.003 to 0.1 % resulted in a significant rise in selectivity toward the formation of NO_3^- (48.1 % of NO_x oxidation) and reduction of NO_2 levels. The improvement in the NO_x oxidation activity was attributed to the presence of grafted iron ions, which enhanced the production of oxidizing species such as hydroxyl radicals. In contrast, Wu and Van de Krol [9,13] investigated TiO_2 modified by oxygen vacancies (O_v) and iron doping. Initially, they employed a thermal pyrolysis method under a reducing atmosphere to

* Corresponding author at: Department of Chemistry, Università degli Studi di Milano, Via C. Golgi 19, 20133 Milano, Italy.
E-mail address: ermelinda.falletta@unimi.it (E. Falletta).

https://doi.org/10.1016/j.jphotochem.2024.115805
Received 18 March 2024; Received in revised form 15 May 2024; Accepted 31 May 2024
Available online 6 June 2024

introduce a large concentration of O_v in TiO_2. This resulted in enhanced photo-oxidation of NO to NO_2 compared to bare TiO_2. Interestingly, the photoreduction process was also observed, contributing to the production of N_2 and O_2. This phenomenon was likely attributed to the O_v, which serves as an active center by capturing NO molecules and participating in the photoreduction reaction. Furthermore, the introduction of Fe^{3+} ions influenced the reaction mechanism in two different ways. Firstly, they act as stabilizers for O_v through charge compensation, thereby facilitating electron transfer processes and improving the performance of photoreduction reactions. Secondly, Fe^{3+} ions can undergo reduction to Fe^{2+}, stabilizing the recombination pathway that suppresses the formation of NO_2, thus favoring the selectivity toward N_2 formation. Despite the efficiency remaining modest, the Fe/TiO_2 catalysts did not exhibit signs of deactivation.

The investigation into alternative elements, such as N, C, F, B, S, and P, for modifying the TiO_2 lattice modification aims to enhance light absorption in the visible spectrum. This exploration was prompted by challenges associated with metal doping, including additional recombination centers and diminished thermostability. Tseng *et al.* [9,14] prepared C-modified TiO_2 structures through an impregnation method, where the authors used anatase TiO_2 and ethanol as raw materials. The carbon-modified TiO_2 at 200 °C catalyst exhibited the fastest NO removal rate, which was associated with a large content of carbon (18.3 %) that facilitates electron conduction and reduces e^-/h^+ pairs recombination. On the other hand, Tobaldi *et al.* [9,15] fabricated N-modified nano TiO_2 (10 nm) via a green aqueous sol–gel method, followed by a thermal treatment between 450 °C and 800 °C. The most efficient catalyst was N-modified anatase TiO_2 calcined at 450 °C, prepared with ammonia as a nitrogen source. This catalyst exhibited doubled NO_x photocatalytic activity compared to P25 under white-light lamp irradiation. The enhancement was ascribed to nitrogen integration into the TiO_2 lattice, generating mid-gap states. However, at higher thermal treatment temperatures a phase transformation to rutile and an increase in crystalline domain size occurred, reducing the surface area and stability of nitrogen in the TiO_2 lattice. Consequently, this adversely affected detrimentally the NOx photocatalytic activity.

In the pursuit of designing TiO_2-based photocatalysts with high visible light absorption, coupling TiO_2 with certain metal oxides has emerged as a promising strategy [9]. For instance, TiO_2-Al_2O_3 was successfully synthesized by Soylu *et al.* [16] via the sol–gel method. In this composite, TiO_2 served as the photocatalyst for NO oxidation with O_2, whereas Al_2O_3 sites were utilized for NO_x storage. The 0.5 TiO_2/Al_2O_3 photocatalyst, calcined at 900 °C, demonstrated a 160 % increase in NO_x storage and a 55 % decrease in NO_2 release in comparison to Degussa P25. This enhancement could be attributed to a unique crystallographic mixture of anatase and rutile phases, as well as a narrow energy band gap achieved under at the synthesis conditions. On the other hand, WO_3/TiO_2 [17] and Fe_2O_3/TiO_2 [18] have been other composites with excellent efficiency for NO_x photo-oxidation. In the former, Luévano-Hipolito *et al.* [19] prepared WO_3/TiO_2 composites through co-precipitation method followed by a thermal treatment at 500 °C for 24 h. Excellent photocatalytic results, with an 80 % conversion of NO conversion under visible light, using a WO_3/TiO_2 sample containing 80 % anatase TiO_2 and 20 % monoclinic WO_3. The enhanced photocatalytic activity was attributed to the synergistic effect between the two photocatalysts. Particularly, TiO_2 facilitate the adsorption of NO molecules on its surface, whereas e^-/h^+ were photogenerated in WO_3 and due to its narrow energy band gap, the electron transfer was promoted efficiently. On the other hand, the latter study was performed by Balbuena *et al.* [18] where Fe_2O_3/TiO_2 nanocomposites were fabricated using a plasma enhanced-chemical vapor deposition (PE-CVD)/radio frequency (RF) sputtering approach and further tested towards NO_x photocatalytic abatement under solar illumination. The individual photocatalytic activities of bare Fe_2O_3 and TiO_2 were found to be negligible. This was associated with hematite's fast recombination, which led to diminished concentrations of hydroxyl radicals (•OH), and TiO_2's large band gap, respectively. Whilst, the formation of Fe_2O_3/TiO_2 junction particularly improved de-NO_x efficiency by facilitating the separation of charge carriers and extending their lifetime.

Furthermore, noble metals nanoparticles (Ag, Au, Pd and Pt) in contact to TiO_2 have demonstrated to remarkable efficiency as photocatalysts toward NO_x degradation [9]. Among these metals, Ag is regarded as a low-cost material in comparison to Au, Pt or Pd metals, while also displays a higher stability against oxidation compared to Cu. Wang *et al.* [20] prepared plasmonic Ag-TiO_{2-x} composites using a simple photochemical reduction method, followed by a post-annealing treatment in Ar gas flow at 250 °C for 2 h. This treatment promoted the generation of oxygen vacancies and Ti^{3+} states. The Ag-TiO_{2-x} composites exhibited approximately 45 % NO removal under visible light irradiation and reduced NO_2 release gas concentrations. The improved NO photocatalytic efficiency was attributed to the synergistic effect between Ag nanoparticles (NPs) and O_v. Initially, the LSPR effect of Ag NPs facilitated the generation of "hot electrons", which overcame the Schottky barrier formed by the interaction between Ag NPs and TiO_2. These transferred "hot electrons" left positive charges at the Ag NPs, actively participating in the NO photo-oxidation process. This mechanism promoted charge carrier separation and extended the lifetime of photo-generated electron-hole pairs. In addition, the presence of O_v created catalytic centers that enhanced the selectivity of the NO_2 degradation pathway toward N_2 and O_2 (photo-reduction process). In further studies, the authors investigated Ag nanoclusters (Ag NCs) smaller than 2 nm on TiO_2 for NO photocatalytic degradation [21]. Interestingly, a molar ratio of 0.89 % in Ag/Ti was necessary to achieve 62 % NO removal within 7 min. This achievement represents a significant improvement, being 3 times higher compared to the efficiency observed with bare TiO_2. In this instance, the absence of the LSPR effect in the wavelength range of 380–420 nm was attributed to the small size of the Ag NCs. However, the electron transfer to the TiO_2 conduction band and promotion of charge carrier separation persisted, contributing to the improvement of NO photocatalytic efficiency. By the electron paramagnetic resonance (EPR) measurements and scavenger tests it was confirmed that the $\bullet O_2^-$ radicals played a key role in the NO photo-oxidation process (NO_3^- formation).

Bearing in mind the diverse families of semiconductors and other complex systems beyond TiO_2-based photocatalysts [9,17] for photocatalytic NO removal, extensive research exists in the literature exploring alternative options, such as hierarchical porous g-C_3N_4 [22], Ag/g-C_3N_4 [9], ZIF-67/CoOOH modified g-C_3N_4 [23], Bi/g-C_3N_4 [24], rGO/Fe-g-C_3N_4 [24], Eu^+-doped layered double hydroxide (LDH) [25], C particles over Bi_2WO_6/TiO_2 (Z-scheme heterojunction) [26], and CdS/$Na_2Ti_3O_7$ [27]. A novel class of photocatalysts, perovkite oxides, comprises a diverse range of compounds characterized by the general formula ABO_3. Initially, they were well-recognized for their promising role in water splitting application [28]. Nevertheless, recent investigations have expanded their scope to environmental remediation as well [29]. In particular, strontium titanate ($SrTiO_3$, STO) is a cubic perovskite-type semiconductor, inexpensive with high thermal stability, corrosion resistance, and a similar energy band gap to TiO_2 (3.2 eV) [30]. As well as TiO_2, STO absorbs under UV irradiation, which represents less than 5 % of the total solar spectrum [7]. Therefore, strategies similar to those already developed for TiO_2 to extend the absorption within the visible part of the electromagnetic spectrum can be applied, for instance by the addition of plasmonic nanoparticles [31–33].

As a first approach, Ma *et al.* [34] prepared Ag-NPs onto STO (1 0 0) surface for the degradation of methylene blue under UV and visible light, whereas Xian *et al.* [35] deposited Ag NPs with a size range 5–15 nm onto $SrTiO_3$ particles via photocatalytic reduction method for the degradation of acid orange under UV irradiation, noticing excellent photocatalytic activity when the highest Ag loading amount was employed.

On the other hand, lattice distortion in semiconductors by the incorporation of foreign elements, called dopants, is a commonly

practiced modification strategy for improving STO photocatalytic performance due to the formation of new energy levels among the conduction and valence band of the host material [36]. In this regard, Subramanian *et al.* [37] studied the modification of STO by using noble-metals (Ag, Pt or Au) *via* an adjusted Pechini procedure. The as-prepared photocatalysts samples were tested for the degradation of Victoria Blue dye under UV–visible light and Ag-$SrTiO_3$ exhibited the best performance (1.0 wt% Ag loading). Moreover, in our previous work [38], the effect of the double modification of STO surface and STO structure with Ag NPs and Ag ions, respectively, via an one-pot solution synthesis was highlighted. The combined effect between these two modifications demonstrated highly photocatalytic efficiency by achieving thorough nitrogen oxides degradation within 180 min.

To the date, in literature there are few investigations concerning the potential ability of the noble metal-decorated $SrTiO_3$ materials towards NO_x degradation. For example, it is reported the fabrication of one-pot plasmonic Ag-STO nanocomposites towards the degradation of NO under visible light, demonstrating that 0.5 wt% Ag-STO led to the best performance with nearly 30 % NO abatement within 30 min [39]. Similarly, Ma *et al.* [40] synthesized an Ag-STO material through a hydrothermal method followed by photochemical reduction. The 15 % Ag-STO (molar ratio) photocatalyst demonstrated 19.6 % more of photoactivity (70 % of NO photodegradation) under visible light within 30 min in comparison to bare STO (50.4 % of NO photodegradation). The enhancement was attributed to LSPR effect of Ag nanoparticles combined with the incorporation of oxygen vacancies. In this work, we report a facile and low waste stream method for the decoration of $SrTiO_3$ by Ag NPs leading to Ag@STO characterized by an extraordinary high activity towards NO_x degradation under LED irradiation. Moreover, it is assessed and discussed the size effect of STOs on their photocatalytic properties.

2. Materials and methods

2.1. Chemicals

Two commercial strontium titanates with different size particles were purchased from Sigma-Aldrich (Italy): micrometric strontium titanate (>99 %) and nanometric strontium titanate (nanopowder < 100 nm, 99 %). They were labelled as STOm and STOn, respectively. In addition, KNO_3 (≥99.0 %), polyvinylpyrrolidone (PVP), HNO_3 (ACS reagent, 70%), and acetone (HPLC grade, ≥99.0 %) were provided by Sigma Aldrich (Italy). All chemicals were used without further purification. An Ag^+-enriched aqueous solution was obtained from Argor-Heraeus SA (Mendrisio, Switzerland), its composition is described in Table 1 [38].

2.2. Synthesis of Ag@STO materials

Ag@STOm and Ag@STOn were synthesized following the procedure previously described elsewhere [41]. Briefly, the photocatalysts were prepared by wet impregnation method. 5 g (27 mmol) of commercial STO (STOm and STOn) were suspended separately in 6 mL of acetone for 30 min at room temperature (*ca.* 24 °C). Then, 13 mL of a 30 g/L solution of Ag NPs, previously synthesized by an electrochemical method starting from the Ag^+-enriched wastewater, as described in the Appendix, were added [41,42]. The mixture was stirred at 40 °C for 24 h at 36 rpm in air. Afterwards, the solvent was vacuum-evaporated by a rotavapor (Strike 300, Steroglass) at 60 °C and the photocatalysts were dried overnight at 110 °C in air. Then, all the materials were calcined at a unique temperature (400 °C) in air atmosphere adopting the following ramp (8 °C/min from 50 to 100 °C, time 30 min; 8 °C/min from 100 to 200 °C, time 30 min; 8 °C/min from 200 to 400 °C, time 120 min) and then quenched at room temperature. For comparison, pristine STOm and STOn were calcined at 400 °C, as well.

2.3. Characterization

X-ray diffraction (XRD) patterns were collected at room temperature on a Rigaku-Miniflex-600 diffractometer using Cu- Kα radiation (λ = 1.541874 Å) at a scan rate of 0.02° min to determine the crystal structure. Silicon (powder) NIST 640f was used to correct instrumental broadening. The morphology of the synthesized photocatalysts were studied by scanning electron microscopy (SEM) operating with a Field Emission source (model TESCAN S9000G; Source: Schottky type FEG; Resolution: 0.7 nm at 15 keV (in In-Beam SE mode, Brno – Kohoutovice, Czech Republic)). The surface areas of the samples were determined by BET adsorption method on a Micromeritics Tristar II 3020 Analyzer. Samples were treated at 150 °C for 4 h under nitrogen flow (Air Liquid, Alphagaz, >99.9 % pure). UV–Vis Diffuse reflectance spectra were collected at room temperature on a Perkin Elmer Lambda 35 UV–Vis Spectrometer equipped with an integrating sphere. The data collected was converted using Kubelka-Munk formula. Fourier transform infrared (FT-IR) spectra were carried out on a PerkinElmer Spectrum

100 spectrometer (Waltham, MA, USA), in 400–4000 cm^{-1} range at room temperature. Before the analysis the samples were dried at 120 °C overnight. Lastly, X-ray photoelectron spectroscopy (XPS) measurements were performed on a M-probe apparatus equipped with Al Kα source ($h\nu$ = 1486.6 eV). Survey scans were measured between 0 and 1100 eV binding energy range with 5 eV energy resolution. All the binding energies were referenced to C1s peak at 284.6 eV of surface adventitious carbon.

2.4. Photocatalytic activity tests

Each sample (50 mg) was suspended in 5 mL of isopropanol (Technical grade, Sigma-Aldrich) and mixed in an ultrasound bath for 2 min. Then, a thin film of the photocatalyst was formed depositing the suspension on a glass plate (3.3 cm × 11.5 cm) by drop-casting method. Once the solvent was evaporated, the photocatalyst was placed inside a 20L Pyrex glass cylindrical batch reactor filled with NO_x. The initial concentration of NO_x was 500 ± 50 ppb. The photocatalytic tests were carried out at 25 °C for 3 h under LED light (350 mA, 9–48 V, 16.8 W) with an emission range of 400–700 nm yielding an effective intensity of 2900 lx on the catalyst surface. The NO_x concentration was measured after 30, 60 and 180 min of irradiation by a chemiluminescence analyzer (ENVEA AC32e). The photolysis test result was nearby 10 % of pollutant degradation after 3 h of light irradiation (Fig. S1).

Based on the ISO 22197-1:2016 rules (ISO 2016) [43], where 1 ppm of NO_x is degraded under UV light, here the photodegradation of 500 ppb of NO_x was explored for three main reason: i) reducing the pollutants concentration compared to the ISO method, as real indoor pollution is typically present at concentrations of only a few parts per billion (ppb),ii) stressing the photocatalysts performance in hard conditions, iii) being able to carry out kinetic investigations (lower NO_x concentrations would lead to fast photodegradation reactions, hard to be investigated from a kinetic point of view).

The most performing photocatalyst (Ag@STOn) was subjected to

Table 1
Composition of Ag^+ enriched solution (mg/L).

Au	Ag	Pd	Cd	Cu	Fe	Ni	Pb	Se	Zn	Te	Al	SO_4^{-2}	Others metals
1.3	267,000	15.2	9	7446.9	16.6	383.2	341.7	2.1	130.8	5.7	2.6	420	<1

three recycle tests without any post-treatment. At the end of each run, the Ag@STOn-loaded glass plate was removed from the Pyrex glass cylindrical batch reactor, stored in the dark in the air at room temperature (*ca.* 24 °C) for one night, and then reused.

3. Results and discussion

The synthesized photocatalysts consisted in two commercial STO having different particles size (micrometric STO, STOm, and nanometric STO, STOn), and the corresponding Ag NPs decorated STOs (nominal 8 wt% of Ag), Ag@STOm and Ag@STOn. The two Ag NPs-modified STO were properly prepared and extensively characterized. All the materials were employed for NO_x degradation under LED irradiation.

3.1. Characterization

The XRD patterns of the samples are depicted in Fig. 1. Pristine STOm and STOn exhibited the characteristic diffraction peaks related to (1 0 0), (1 1 0), (1 1 1), (2 0 0), (2 1 0), (2 1 1), (2 2 0) and (3 1 0) planes located at 22.7°, 32.4°, 40.0°, 46.6°, 52.3°, 57.8°, 68.0° and 77.3°, respectively,- indicating the cubic crystal structure with space group of Pm-3m (JCPDS: 01-084-0443) [44]. Nevertheless, traces of a second phase corresponding to Sr_2TiO_4 are observed in the STOm diffraction pattern (Fig. 1b). This structure presents two strong intense peaks located at 31.4° and 32.6°, which are assigned correspondingly to (0 1 3) and (1 1 0) planes. In the diffractograms, only the plane (0 1 3) can be slightly noticed since the plane (1 1 0) is overlapped by the plane (1 1 0) at the 32.4° of $SrTiO_3$ [45,46]. The presence of Sr_2TiO_4 is attributable to the synthetic approach used for the commercial STO synthesis and/or to the calcination temperature.

On the other hand, both Ag@STOm and Ag@STOn samples showed additional peaks at 38.1°, 44.4°, and 64.4°, distinctive of metallic Ag. The average crystallite size (D) was calculated by the Scherrer Equation (Eq. (1)), using as shape factor $k = 0.9$. λ is the X-ray wavelength Cu(kα), and B_{hkl} is the full width at half maximum (FWHM) in radian, whereas θhkl is the diffraction angle. The peaks at 32.4° for $SrTiO_3$ and 38.04° for Ag that belongs to 1 1 0 and 1 1 1 reflections, respectively, were used for the estimation.

$$D = \frac{k\lambda}{\beta_{hkl} Cos\theta_{hkl}} \quad (1)$$

Based on the results shown in Table 2 and compared to the bare STO samples, it can be seen that there were not structure changes during the decoration step [47,48].

The porosity and surface area of the photocatalysts were studied using N_2 adsorption–desorption isotherm measurements. As it can be seen in Fig. 2, all the photocatalysts can be classified as non-porous materials and the isotherms belong to type–II, according to IUPAC classifications [49]. The specific surface area (SSA), pore size and pore volume of all the photocatalysts are reported in Table 2, and as expected, it is higher for nano-sized structures (almost an order of magnitude) than for micrometric ones. Moreover, the STOn-based materials showed pores sized twice as large as those of the corresponding STOm materials, and 19 times the pore volume.

To investigate the morphology of the photocatalysts, both the Ag-decorated and bare STO compounds were also analyzed by FESEM (Fig. 3). The bare STOm material (as reported in Fig. 3a) exhibited agglomerated and cubic-like morphology with a particle size in the 0.4–0.7 μm range. The Ag@STOm photocatalyst (Fig. 3b) showed well-dispersed Ag NPs (sphere-shaped with diameter of 0.3–0.7 μm) onto the surface of STOm. On the other hand, the commercial STOn surprisingly consists in hierarchical microspheres (~50 μm) organized in self-assembly nano-sized cubes in the 30–40 nm size range (Fig. 3e) [50,51]. In addition, in the Ag@STOn spherical Ag NPs with a 0.5 μm mean size were successfully deposited onto the STOn hierarchical microsphere surface. Lastly, further analysis by EDS (Fig. 3d and h) confirmed the elemental composition for both Ag@STO samples. The Ag NPs were found much better dispersed onto STOn than onto STOm, suggesting that hierarchical structures benefit the distribution of Ag micro-sized particles onto its surface. The Ag weight percentage in Ag@STOm and Ag@STOn was 7.1 % and 7.9 %, respectively (Fig. 3). Moreover, both samples exhibited the presence of Cu which derived from the Ag^+-enriched solution (Figs. S2 and S3).

In order to identify the functionalities present in both bare STO and Ag@STO samples, FT-IR spectra were performed in the 400–4000 cm^{-1} frequency range (Figs. S4 and S5). The spectra exhibit several bands at 410 cm^{-1}, 611 cm^{-1}, 859 cm^{-1}, 1464 cm^{-1}, 1630 cm^{-1}, 2360 cm^{-1}, and 3444 cm^{-1}. The bands at 410 cm^{-1} and 611 cm^{-1} are assigned to vibrational modes of Ti-O band [52,53]. On the other hand, the absorption bands at 859 cm^{-1} and 1464 cm^{-1} are due to the presence of carbonates species [53,54]. The band at 2360 cm^{-1} corresponds to C═O stretching from adsorbed CO_2 [55]. In addition, the presence of spectral components located at $\nu > 3400$ cm^{-1} indicates that a certain amount of hydration is evident, in particular, because it is coupled with the band centered at *ca.* 1630 cm^{-1}. These spectral components are counterparts related to the presence of OH/H_2O species [56]. In particular, for the Ag@STOn composite, the high frequency mode is characterized by a moderate intensity, which indicates a medium-to-high hydration degree of its surface. The absorption bands of Ag@ STO samples are quite similar compared to the pristine STO materials. This permits to conclude that the decoration of STO surface by Ag micro-sized particles did not

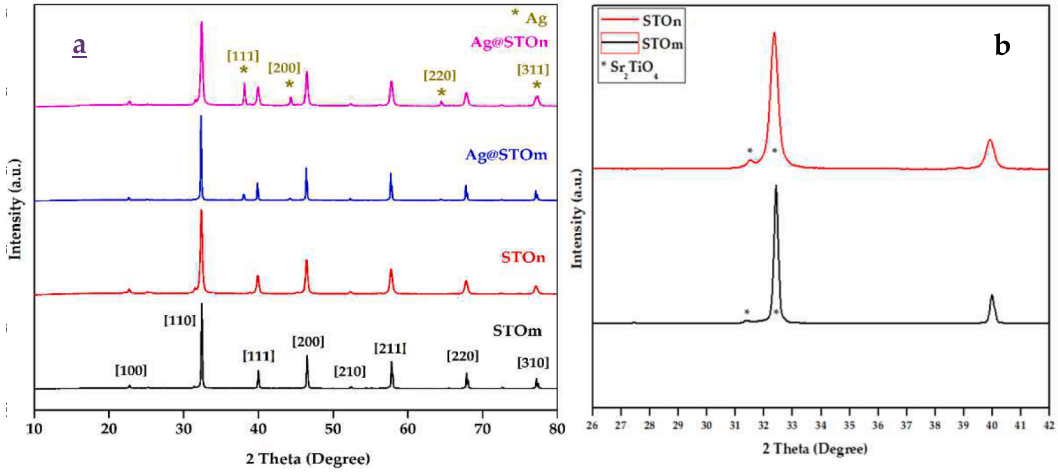

Fig. 1. (a) XRD patterns of bare STOm and STOn and the corresponding Ag NPs decorated ones, (b) Magnification of STOm and STOn XRD pattern and Sr_2TiO_4 phase highlighted.

Table 2
Crystallite size, Specific surface area (SSA), pore size, pore volume, energy bandgap values and rate constants of the photocatalysts.

	Crystallite size STO (nm)	Crystallite size Ag (nm)	BET surface (m^2/g)	Pore Size (nm)	Pore Volume (cm^3/g)	Band gap (eV)	Constant rate (min^{-1})
STOm	545	–	2	11	0.0065	3.2	0.0009
STOn	53	–	22	25	0.1505	3.2	0.0028
Ag-STOm	493	183	2	12	0.0063	3.2	0.0018
Ag-STOn	55	172	17	29	0.1207	2.9	0.0079

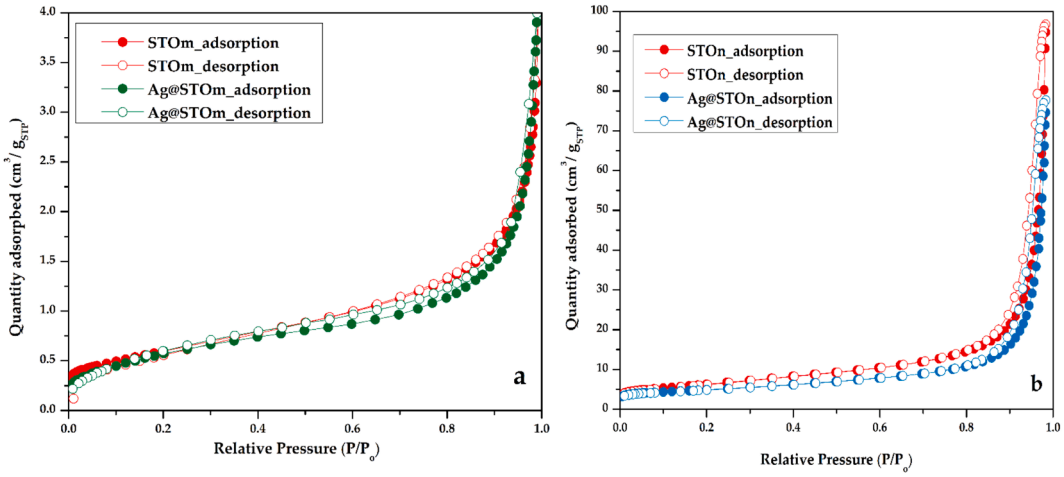

Fig. 2. Nitrogen adsorption–desorption isotherms of (a) STOm and Ag@STOm and (b) STOn and Ag@STOn.

produce any specific change on the STOn structure, in accordance with the XRD patterns.

The surface elemental composition and chemical states of STOs and the corresponding Ag-decorated samples were studied by XPS. The survey spectra confirmed the presence of Sr, Ti, O, C, and Ag for the modified materials (Table S1, Figs. S6–S9). All the binding energies were calibrated to C1s peak at 284.6 eV, which is ascribed to adventitious carbon. The high-resolution spectra of Sr, Ti, O, and Ag species for Ag@STOn sample are displayed in Fig. 4a–d, whereas those of pristine STOs and Ag@STOm are reported in Figs. S10–S12. Focusing the attention on the STOn-based photocatalysts, in Fig. S10a it is possible to observe in the HR spectrum of Sr of STOn two binding energy peaks at 133.5 eV and 135.3 eV, corresponding to $3d^{5/2}$ and $3d^{3/2}$, respectively, in accordance to $SrTiO_3$ [57].

The HR spectrum of Ti 2p (Fig. S10b) exhibits a doublet at 459.3 and 464.8 eV associated to Ti 2p 3/2 and 1/2 components of Ti^{4+} and a second doublet at 457.5 and 462.8 eV due to the presence of Ti^{3+} species. The splitting orbital energy between these two peaks is *ca.* 5.7 eV, which confirms the presence of Ti^{4+} species [58].

Concerning the HR spectrum of O1s (Fig. S10c), it is evident the presence of two peaks at values of binding energy equal to 527.7 and 528.8 eV that can be attributed to the lattice oxygen ion and oxygen vacancy, whereas the other two peaks centered at 530.1 and 531.6 eV are associated to the adsorption of OH species on the STO surface. Similar results were obtained for STOm, as shown in Fig. S11.

Similarly to STOn, the HR spectrum of Sr of Ag@STOn shows two binding energy peaks at 133.0 eV and 134.9 eV, corresponding to $3d^{5/2}$ and $3d^{3/2}$, respectively, which is in accordance to $SrTiO_3$ [57]. In the high-resolution spectrum of Ti 2p, four binding energy peaks are evidenced. Two peaks centered at the binding energies of 459.7 eV and 465.3 eV are attributed to Ti $2p^{3/2}$ and Ti $2p^{1/2}$ respectively. Whilst, the position of the Ti $2p_{3/2}$ peak at 457.4 eV and the shoulder at 462.9 eV indicate the presence of Ti^{3+} oxidation state [59]. In addition, as shown in Fig. 4c, the O 1s XPS spectrum of Ag@STOn can be divided into three peaks: at 528.8 eV, 530.9 eV, and 533.2 eV corresponded to lattice oxygen, oxygen vacancies, and chemically adsorbed oxygen, respectively [59–61]. Fig. 4d shows the high-resolution spectrum of Ag 3d in which the peaks located at 369.7 eV and 375.7 eV correspond to metallic silver. The latter is confirmed by the splitting orbital energy between Ag $3d_{5/2}$ and Ag $3d_{3/2}$ peaks of 6.0 eV [40]. Whilst, the two subpeaks located at 368.0 eV and 373.9 eV are attributed to the presence of Ag_2O [62]. Moreover, considering as reference the values reported by Galloni *et al.*, it is worth noting that the peak positions of Sr 3d, Ti 2p, O 1s on both samples Ag@STOm and Ag@STOn are shifted towards higher binding energies [63], as a result of the creation a new coordination environment of STO due to Ag NPs and their strong interaction [40,64]. Lastly, the surface Ag atomic amount in the Ag@STOm and Ag@STOn was equal to 1.7 % and 2.5 % of Ag (Table S1), respectively, which might influence the photocatalytic properties.

In order to study the optical properties of pristine STO and Ag@STO samples, UV-DRS analyses were performed, and the results are illustrated in Fig. 5(a and b). As expected, the pristine STOm and STOn samples exhibited low absorbance values in the visible part of the electromagnetic spectrum since they were white powders (Fig. 5a). In contrast, the Ag@STO structures (gray-colored powders) presented high absorbance values in the visible range, which could be attributed to the LSPR effect of Ag NPs [60,65]. In addition, the energy band gap was estimated by plotting the Kubelka Munk function versus incident photon energy (Fig. 5b) [66] and the values are reported in Table 2. The band gap values of the bare samples were found to be 3.2 eV and are in good agreement with previous studies [63]. After Ag NPs decoration, the energy band gap of Ag@STO materials did not change significantly (3.2 eV and 2.9 eV for Ag@STOm and Ag@STOn, respectively) [67,68]. More in detail, Ag@STOn showed the highest absorbance among the STO-based photocatalysts which is mainly attributed to the Ag nanoparticles due to LSPR effect, but also owing to a larger surface area than Ag@STOm sample, and light scattering properties of hierarchical structures [69,70].

3.2. Photocatalytic activity

The photocatalytic activity of the STOs and Ag@STOs materials was evaluated towards the degradation of NO_x (500 ppb) under LED irradiation. As shown in Fig. 6a, after 180 min of irradiation, STOn

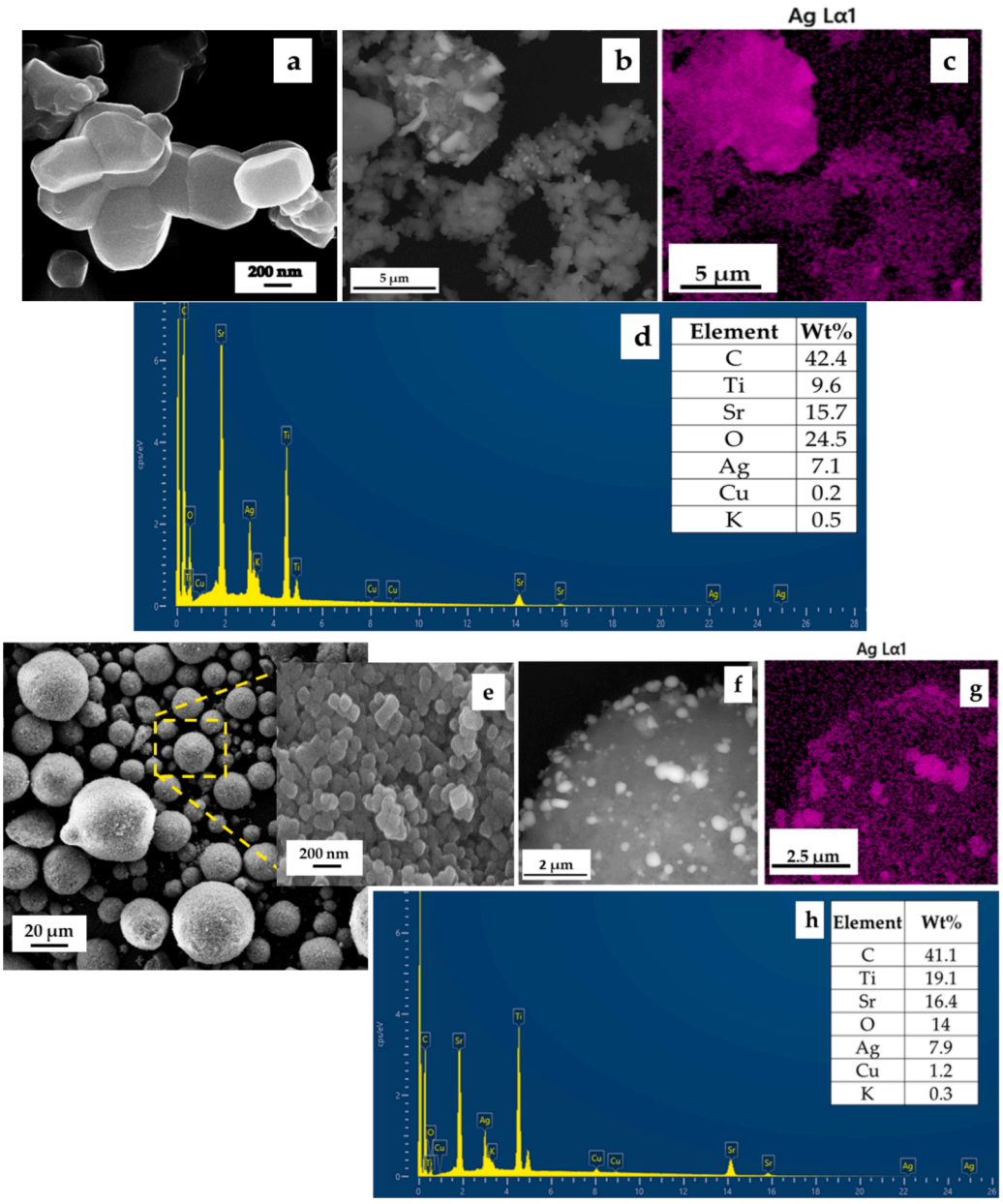

Fig. 3. FESEM images of STOm (a), STOn(e), Ag@STOm (b), Ag@STOn (f), Ag mapping of Ag@STOm (c) and Ag@STOn (g), EDS spectra of Ag@STOm (d) and Ag@STOn (h).

exhibited higher photoactivity (27 ± 3 %) in comparison to STOm (15 ± 3 %), which can be reasonably attributed to the large surface area of the 3D hierarchical structure that not only provides great adsorption of inorganic pollutants but also improves uniformly distribution of active sites, where the production of reactive oxygen species (ROS) and NO_x photodegradation takes place [69,71]. The presence of the second phase (Sr_2TiO_4) does not seem to affect the photocatalytic properties of the materials. In fact, preliminary investigations, carried out using Sr_2TiO_4 (data not shown) as a photocatalyst for NOx abatement, revealed that this latter exhibits a photocatalytic activity very similar to STO.

The decoration of STO samples with Ag NPs boosted up the photoactivity (Fig. 6a). If on one hand, Ag@STOm was able to degrade ca. 40 % of NO_x after 180 min, on the other hand the results obtained by Ag@STOn were very interesting: 75 % within 3 h of irradiation. It is evident that the enhancement of the photocatalytic activities of both the Ag-modified material is linked to the LSPR effect of Ag NPs and the development of Ag@STO heterostructures, which can suppress the faster recombination of photo-generated charge carriers [60,67]. Despite the difference on the amount of Ag loaded onto STOm and STOn surface and the difference between the materials in terms of particles dimensions, it is worth noting that for both STO the Ag NPs decoration caused a photocatalytic enhancement of 2.6 times compared to the corresponding bare perovskite oxides. Meanwhile, the photoactivity of Ag@STOn is 1.8 times higher than of Ag@STOm. This could be explained by the large amount of Ag observed onto STOn surface (2.5 %), and the light-scattering effect that hierarchical structures provide (STOn microsphere), in which the hot-electrons generated in the Ag large particles caused the scattered photons. In such way, hot-electrons receive the necessary energy to be transferred the conduction band of STOn. A proof of it is the lowest absorbance of STOn absorbance (i.e. the highest diffuse reflectance intensity) [70].

The effect exerted by the traces of copper present in the Ag^+-enriched solution on the catalytic activity of the Ag-modified materials deserves a separate discussion.

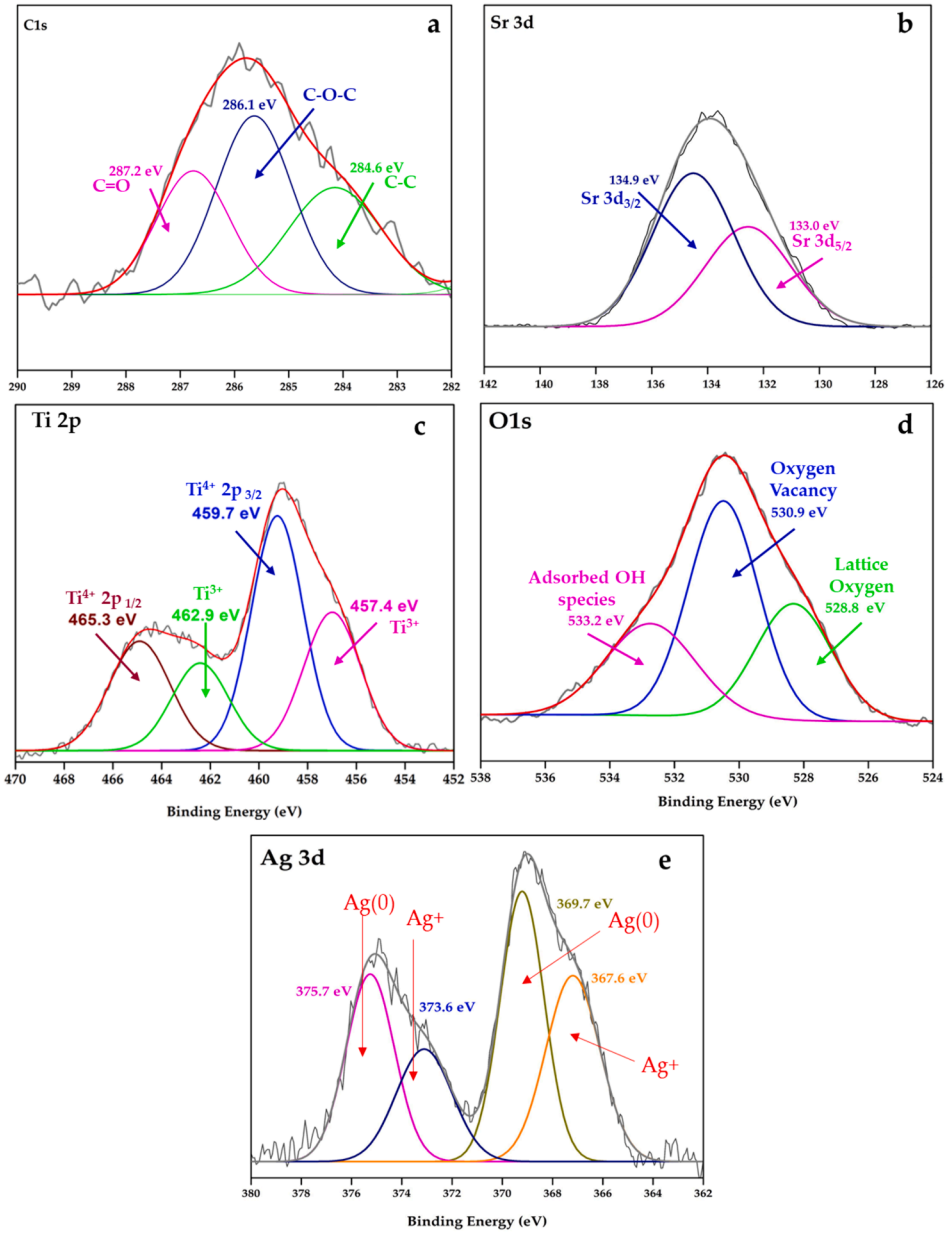

Fig. 4. XPS HR spectra of Sr, Ti, O, and Ag of Ag@STOn.

In a previous work [38], we observed that when Ag@STO is prepared by a one-pot approach, adding the Ag^{+}-enriched solution as metal precursor during the STO synthesis, the presence of metallic contaminants (mainly copper) in the waste solution negatively affects the photocatalytic activity of the final photocatalyst. In contrast, when Ag is introduced in form of nanoparticles by a second step (after the STO synthesis), the photocatalyst maintains high activity towards NO_x abatement. On the other hand, using different semiconductors (TiO_2), the enhanced photocatalytic efficiency was associated to the presence of Cu [72].

Therefore, it is possible to conclude that if Cu species come into the STO structure affecting its ionic structure, as it probably occurs during the Ag@STO one-pot synthesis, the effect on the photocatalyst efficiency is negative. In contrast, according to the literature [72–74], when added as external particles or ions, they are beneficial enhancing the visible light absorption of the material.

Fig. 6b suggests that the degradation of NO_x by all the tested photocatalysts follows first-order kinetics and the estimated rate constants (with regression coefficient ranged from 0.97 to 0.99) are tabulated in Table 2. The most performing material, Ag@STOn, that showed the fastest photodegradation rate, was tested in terms of stability by reusing it for three consecutive cycles without any post-treatment. The results are depicted in Fig. 6c. Despite a slight reduction in activity during the three cycles, the material maintained a good stability, as confirmed by the FT-IR and XRD analyses carried out on the used material (Figs. S13 and S14).

According to Zheng *et al.* [69], the mechanism of reaction of hierarchical microsphere structures relies on the light their scattering properties, where the photons that are not absorbed can be scattered within heterostructure system giving multiple paths to be reabsorbed. It is worth to bear in mind that our studied heterostructure comprises also large Ag particles, which are also controlled by scattering mechanism [33]. In other words, there is a combined effect between the photons that can be scattered from STOn structure and from Ag micro-sized particles, increasing the probabilities of Ag particles being irradiated. Subsequently, electron/hole pairs proceed to the reactive oxygen species

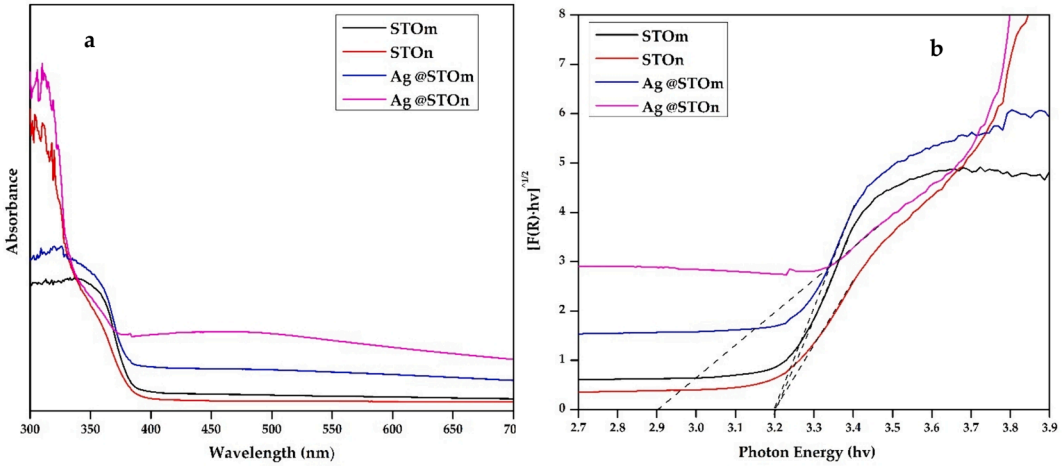

Fig. 5. (a) UV DRS spectra and (b) Tauc of the photocatalysts.

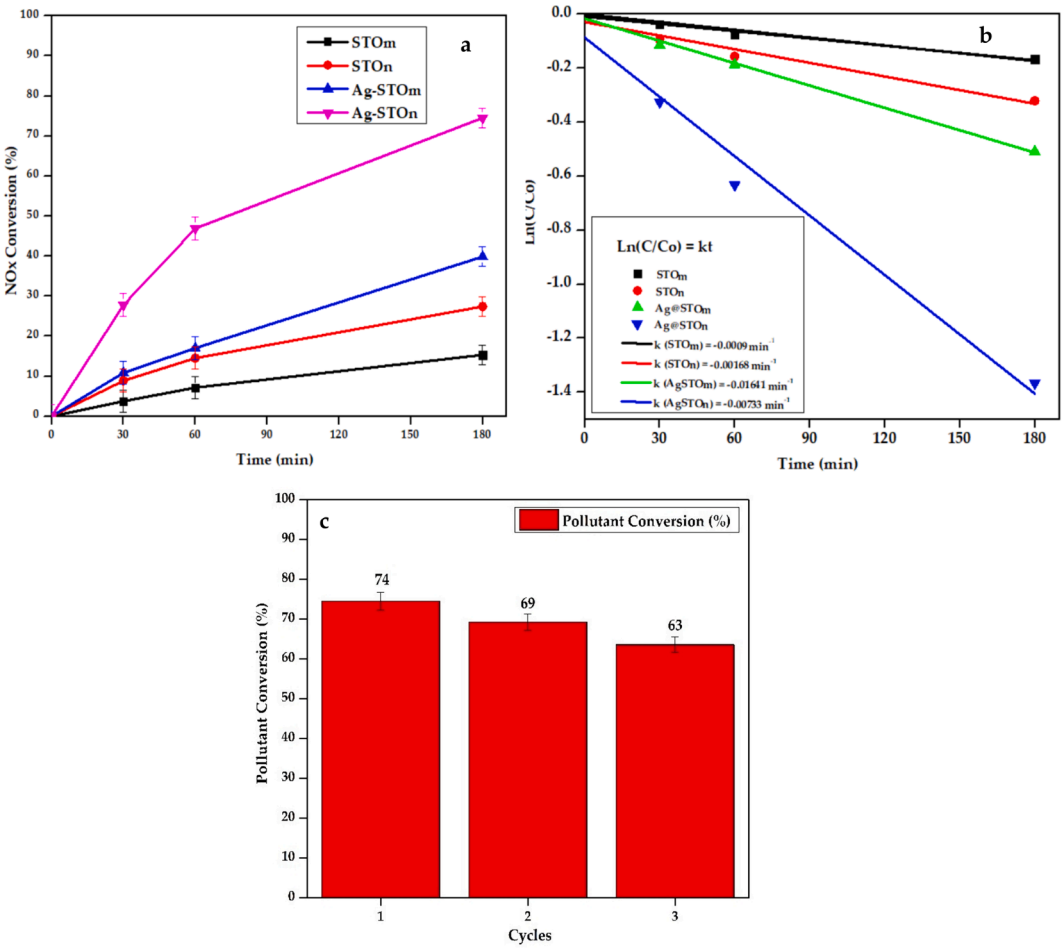

Fig. 6. (a and b) Photocatalytic activity of bare STO and Ag@STO towards NO_x degradation (500 ppb) under LED and (c) Ag@STOn reusability for three cycles without any post-treatment.

(ROS) generation, which are responsible of NO_x degradation process [34,35,65,75]. A scheme of the possible mechanism of reaction can be seen in Fig. 7.

Previous results reported by Zhang *et al.* [39] disclose the synthesis of Ag-STO nanocomposites via one-pot solvothermal method for the degradation of NO under visible light irradiation. The authors demonstrated that the optimal Ag loading 0.5 wt% reached 30 % of NO removal within 30 min. Whilst, by using a multistep approach (hydrothermal method followed by photochemical reduction), a 15 % Ag-STO (molar ratio, equivalent to 9 wt%) composite reached 70 % of NO photodegradation in the same amount of time. In contrast, by using a wet impregnation method for the decoration of STO compounds and an 8 wt % of Ag loading amount, our results went far beyond (75 % of NO_x photodegradation within 180 min). In addition, the STO

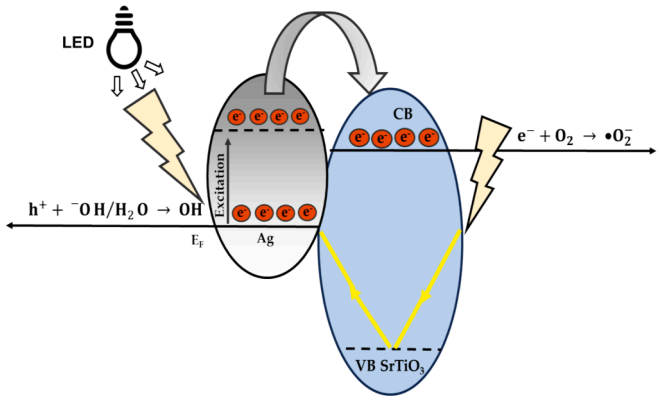

Fig. 7. Schematic illustration of the photocatalytic mechanism of Ag@STOn towards the degradation of NOx.

heterostructures provide a higher surface area (more active sites), uniformly distribution of plasmon particles (avoiding their agglomeration in comparison to Ag@STOm), and the light scattering that increases the chances to irradiate and excite hot electrons (avoiding fast recombination of electron/holes charges). For the first time the surprising scattering properties of Ag@STOn, due to the synergistic effect of the hierarchical microsphere of STO and the micro-sized Ag particles, were reported. For all these reasons, Ag@STOn could be considered a promising safer material and an alternative for air remediation since it is a micro-sized compound with high thermal stability (at 400 °C) and a fast photodegradation activity.

4. Conclusions

In summary, two STOs of different sizes (micro and nano) were decorated by Ag micro-sized particles by wet impregnation method and their photocatalytic activities were tested towards the degradation of NO_x under LED. The XRD characterization confirmed that Ag was deposited onto STO and that no changes in the cubic structure of STO samples occurred, not even after the calcination treatment. Moreover, the photocatalytic experiments reveal the benefits of Ag micro-sized particles deposited onto the two different STO structures. The Ag@STOm photocatalyst, defined by plasmon microparticles onto micro-sized STO cubes, exhibited an agglomerated and heterogeneous system that reflected a low photocatalytic efficiency (40 ± 3 %) within 3 h. On the other hand, since the STOn sample showed a higher photocatalytic efficiency compared to STOm, the addition of Ag microparticles enhanced the photocatalytic activity nearly 2.6 times. Indeed, the Ag@STOn photocatalyst showed an excellent performance towards the degradation of NO_x under LED light (75 ± 3 %) within 3 h, attributed to the combined structure between hierarchical microspheres that were built of nanocubes, Ag large particles, and large amount of Ag on STOn surface (2.5 at.%). Aside from STOn high surface area, this micro-system allows a double light scattering process, due to both STOn and Ag micro-sized particles. Therefore, the potential of irradiation and hot electrons generation is high, enhancing photocatalytic efficiency. Based on these results, Ag@STOn can be proposed as an alternative material for NO_x removal under LED irradiation. Finally, our research highlights the potential of wet impregnation technique as an effective strategy for the development of heterostructures with high performance for nitrogen oxides photodegradation, besides exploiting Ag-enriched solution wastewater as Ag precursor.

CRediT authorship contribution statement

Marcela Frias Ordoñez: Writing – original draft, Methodology, Investigation, Formal analysis, Data curation. **Ermelinda Falletta:** Writing – review & editing, Validation, Supervision, Methodology, Data curation, Conceptualization. **Giuseppina Cerrato:** Writing – review & editing, Formal analysis, Data curation. **Claudia L. Bianchi:** Writing – review & editing, Supervision, Project administration, Funding acquisition, Data curation, Conceptualization.

Declaration of competing interest

The authors declare that they have no known competing financial interests or personal relationships that could have appeared to influence the work reported in this paper.

Data availability

Data will be made available on request.

Acknowledgements

The authors thank Argor-Heraeus SA for providing the Ag^+-enriched solution used for this investigation.

This work was supported by the Department of Chemistry, Università degli Studi di Milano, Italy (Piano Sostegno alla Ricerca, PSR, grant 2022).

This paper has been partly funded by the National Recovery and Resilience Plan (NRRP), Mission 4 Component 2 Investment 1.3—Call for tender No. 1561 of 11.10.2022 of Ministero dell'Università e della Ricerca (MUR) and the European Union—NextGenerationEU, Award Number: Project code PE0000021, Concession Decree No. 1561 of 11.10.2022 adopted by Ministero dell'Università e della Ricerca (MUR), CUP D43C22003090001, Project title "Network 4 Energy Sustainable Transition—NEST".

Appendix A. Supplementary data

Supplementary data to this article can be found online at https://doi.org/10.1016/j.jphotochem.2024.115805.

References

[1] L. Al-Ghussain, Global warming: review on driving forces and mitigation, Environ. Prog. Sustain. Energy 38 (1) (2019) 13–21, https://doi.org/10.1002/ep.13041.
[2] V.-H. Nguyen, B.-S. Nguyen, C.-W. Huang, T.-T. Le, C.C. Nguyen, T.T.N. Le, D. Heo, Q.V. Ly, Q.T. Trinh, M. Shokouhimehr, C. Xia, S.S. Lam, D.-V.-N. Vo, S.Y. Kim, Q. V. Le, Photocatalytic NOx abatement: recent advances and emerging trends in the development of photocatalysts, J. Clean. Prod. 270 (2020), https://doi.org/10.1016/j.jclepro.2020.121912, 121912(1–17).
[3] J. Lasek, Y.H. Yu, J.C.S. Wu, Removal of NOx by photocatalytic processes, J. Photochem. Photobiol. C Photochem. Rev. 14 (1) (2013) 29–52, https://doi.org/10.1016/j.jphotochemrev.2012.08.002.
[4] Z. Shayegan, C.S. Lee, F. Haghighat, TiO_2 photocatalyst for removal of volatile organic compounds in gas phase – a review, Chem. Eng. J. 334 (September 2017) (2018) 2408–2439, https://doi.org/10.1016/j.cej.2017.09.153.
[5] H.S. Russell, L.B. Frederickson, O. Hertel, T. Ellermann, S.S. Jensen, A review of photocatalytic materials for urban nox remediation, Catalysts 11 (6) (2021) 1–45, https://doi.org/10.3390/catal11060675.
[6] A.J. Haider, Z.N. Jameel, I.H.M. Al-Hussaini, Review on: titanium dioxide applications, Energy Proc. 157 (2019) 17–29, https://doi.org/10.1016/j.egypro.2018.11.159.
[7] H.-R. An, S.Y. Park, H. Kim, C.Y. Lee, S. Choi, S.C. Lee, S. Seo, E.C. Park, Y.-K. Oh, C.-G. Song, J. Won, Y.J. Kim, J. Lee, H. U. Lee, Y.-C. Lee, Advanced nanoporous TiO_2 photocatalysts by hydrogen plasma for efficient solar-light photocatalytic application, Sci. Rep. 6 (2016) 29683(1-9). doi: 10.1038/SREP29683.
[8] S. Rehman, R. Ullah, A.M. Butt, N.D. Gohar, Strategies of making TiO_2 and ZnO visible light active, J. Hazard. Mater. 170 (2–3) (2009) 560–569, https://doi.org/10.1016/j.jhazmat.2009.05.064.
[9] B. Rhimi, M. Padervand, H. Jouini, S. Ghasemi, D.W. Bahnemann, C. Wang, Recent progress in NOxphotocatalytic removal: surface/interface engineering and mechanistic understanding, J. Environ Chem. Eng. 10 (6) (2022), https://doi.org/10.1016/j.jece.2022.108566, 108566(1–24).
[10] J. Ma, H. He, F. Liu, Effect of Fe on the photocatalytic removal of NOx over visible light responsive Fe/TiO_2 catalysts, Appl. Catal. B Environ. 179 (2015) 21–28, https://doi.org/10.1016/j.apcatb.2015.05.003.
[11] J. Patzsch, J.N. Spencer, A. Folli, J.Z. Bloh, Grafted iron(iii) ions significantly enhance NO_2 oxidation rate and selectivity of TiO_2 for photocatalytic NOx

abatement, RSC Adv. 8 (49) (2018) 27674–27685, https://doi.org/10.1039/c8ra05017a.
[12] H. Irie, S. Miura, K. Kamiya, K. Hashimoto, Efficient visible light-sensitive photocatalysts: grafting Cu(II) ions onto TiO_2 and WO_3 photocatalysts, Chem. Phys. Lett. 457 (1–3) (2008) 202–205, https://doi.org/10.1016/j.cplett.2008.04.006.
[13] Q. Wu, R. Van De Krol, Selective photoreduction of nitric oxide to nitrogen by nanostructured TiO_2 photocatalysts: role of oxygen vacancies and iron dopant, J. Am. Chem. Soc. 134 (22) (2012) 9369–9375, https://doi.org/10.1021/ja302246b.
[14] Y.H. Tseng, C.H. Kuo, Photocatalytic degradation of dye and NOx using visible-light-responsive carbon-containing TiO_2, Catal. Today 174 (1) (2011) 114–120, https://doi.org/10.1016/j.cattod.2011.02.011.
[15] D.M. Tobald, R.C. Pullar, A.F. Gualtieri, G. Otero-Irurueta, M.K. Singh, M. P. Seabra, J.A. Labrinch, Nitrogen-modified nano-titania: true phase composition, microstructure and visible-light induced photocatalytic NOx abatement, J. Solid State Chem. 231 (2015) 87–100, https://doi.org/10.1016/j.jssc.2015.08.008.
[16] A.M. Soylu, TiO_2-Al_2O_3 binary mixed oxide surfaces for photocatalytic NOx abatement, Appl. Surf. Sci. 318 (2014) 142–149, https://doi.org/10.1016/j.apsusc.2014.02.065.
[17] F. Li, G. Liu, F. Liu, S. Yang, A review of self-cleaning photocatalytic surface: effect of surface characteristics on photocatalytic activity for NO, Environ. Pollut. 327 (March) (2023) 121580(1-16). doi: 10.1016/j.envpol.2023.121580.
[18] J. Balbuena, G. Carraro, M. Cruz, A. Gasparotto, C. Maccato, A. Pastor, C. Sada, D. Barreca, L. Sànchez, Advances in photocatalytic NOx abatement through the use of Fe_2O_3/TiO_2 nanocomposites, RSC Adv. 6 (78) (2016) 74878–74885, https://doi.org/10.1039/c6ra15958c.
[19] E. Luévano-Hipólito, A. Martínez-De La Cruz, E. López-Cuellar, Q.L. Yu, H.J. H. Brouwers, Synthesis, characterization and photocatalytic activity of WO_3/TiO_2 for NO removal under UV and visible light irradiation, Mater. Chem. Phys. 148 (1–2) (2014) 208–213, https://doi.org/10.1016/j.matchemphys.2014.07.034.
[20] Y. Duan, M. Zhang, L. Wang, F. Wang, L. Yang, X. Li, C. Wang, Plasmonic Ag-TiO_2-x nanocomposites for the photocatalytic removal of NO under visible light with high selectivity: the role of oxygen vacancies, Appl. Catal. B Environ. 204 (2017) 67–77, https://doi.org/10.1016/j.apcatb.2016.11.023.
[21] Y. Duana, J. Luo, S. Zhou, X. Mao, M.W. Shah, F. Wang, Z. Chen, C. Wang, TiO_2-supported Ag nanoclusters with enhanced visible light activity for the photocatalytic removal of NO, Appl. Catal. B Environ. 234 (January) (2018) 206–212, https://doi.org/10.1016/j.apcatb.2018.04.041.
[22] Y. Xia, H. Yang, W. Ho, B. Zhu, J. Yu, Promoting the photocatalytic NO oxidation activity of hierarchical porous g-C_3N_4 by introduction of nitrogen vacancies and charge channels, Appl. Catal. B Environ. 344(November 2023) (2024) 123604(1-10). doi: 10.1016/j.apcatb.2023.123604.
[23] G. Dua, Q. Zhang, W. Xiao, Z. Yi, Q. Zheng, H. Zhao, Y. Zou, B. Li, Z. Huang, D. Wang, L. Zhu, ZIF-67/CoOOH cocatalyst modified g-C_3N_4 for promoting photocatalytic deep oxidation of NO, J. Alloys Compd. 882 (2) (2021), https://doi.org/10.1016/j.jallcom.2021.160318, 160318(1–8).
[24] Y. Li, K. Lv, W. Ho, Z. Zhao, Y. Huang, Enhanced visible-light photo-oxidation of nitric oxide using bismuth-coupled graphitic carbon nitride composite heterostructures, Chinese J. Catal. 38 (2) (2017) 321–329, https://doi.org/10.1016/S1872-2067(16)62573-1.
[25] A. Pastor, C. Chen, G. de Miguel, F. Martín, M. Cruz-Yusta, D. O'Hare, I. Pavlovic, L. Sànchez, Facile synthesis of visible-responsive photocatalytic Eu-doped layered double hydroxide for selective removal of NOx pollutant, Chem. Eng. J. 471 (April) (2023), https://doi.org/10.1016/j.cej.2023.144464.
[26] R. Yuan, M. Wang, L. Liao, W. Hu, Z. Liu, Z. Liu, L. Guo, K. Li, Y. Cui, F. Lin, F. Tao, W. Zhou, 100% N_2O inhibition in photocatalytic NOx reduction by carbon particles over Bi_2WO_6/TiO_2 Z-scheme heterojunctions, Chem. Eng. J. 453 (2023), https://doi.org/10.1016/j.cej.2022.139892, 139892(1–10).
[27] W. Dai, S. Zhang, H. Shang, S. Xiao, Z. Tian, W. Fan, X. Chen, S. Wang, W. Chen, D. Zhang, Breaking the selectivity barrier: reactive oxygen species control in photocatalytic nitric oxide conversion, Adv. Funct. Mater. 34 (4) (2024), 2309426 (1–14).
[28] A. Kumar, A. Kumar, V. Krishnan, Perovskite oxide based materials for energy and environment-oriented photocatalysis, ACS Catal. 10 (17) (2020) 10253–10315, https://doi.org/10.1021/acscatal.0c02947.
[29] R. Djellabi, M.F. Ordonez, F. Conte, E. Falletta, C.L. Bianchi, I. Rossetti, A review of advances in multifunctional $XTiO_3$ perovskite-type oxides as piezo-photocatalysts for environmental remediation and energy production, J. Hazard. Mater. 421(May 2021) (2022) 126792. doi: 10.1016/j.jhazmat.2021.126792.
[30] B.L. Phoon, C.W. Lai, J.C. Juan, P.L. Show, G.T. Pan, Recent developments of strontium titanate for photocatalytic water splitting application, Int. J. Hydrogen Energy 44 (28) (2019) 14316–14340, https://doi.org/10.1016/J.IJHYDENE.2019.01.166.
[31] A. Gellé, A. Moores, Plasmonic nanoparticles: photocatalysts with a bright future, Curr. Opin. Green Sustain. Chem. 15 (2019) 60–66, https://doi.org/10.1016/j.cogsc.2018.10.002.
[32] X. Zhang, Y.L. Chen, R.-S. Liu, D.P. Tsai, Plasmonic photocatalysis, Reports Prog. Phys. 76(4) (2013) 046401, 046401(1-41). doi: 10.1088/0034-4885/76/4/046401.
[33] N. Zhou, V. López-Puente, Q. Wang, L. Polavarapu, I. Pastoriza-Santos, Q.H. Xu, Plasmon-enhanced light harvesting: applications in enhanced photocatalysis, photodynamic therapy and photovoltaics, RSC Adv. 5 (37) (2015) 29076–29097, https://doi.org/10.1039/c5ra01819f.
[34] L. Ma, T. Sun, H. Cai, Z.Q. Zhou, J. Sun, M. Lu, Enhancing photocatalysis in $SrTiO_3$ by using Ag nanoparticles: a two-step excitation model for surface plasmon-enhanced photocatalysis, J. Chem. Phys. 143 (8) (2015), https://doi.org/10.1063/1.4929910, 084706(1–7).
[35] T. Xian, H. Yang, L.J. Di, J.F. Dai, Enhanced photocatalytic activity of $SrTiO_3$ particles by surface decoration with Ag nanoparticles for dye degradation, Phys. Scr. 90 (5) (2015), https://doi.org/10.1088/0031-8949/90/5/055801, 055801 (1–8).
[36] C.B. Anucha, I. Altin, E. Bacaksiz, V.N. Stathopoulos, Titanium dioxide (TiO_2)-based photocatalyst materials activity enhancement for contaminants of emerging concern (CECs) degradation: In the light of modification strategies, Chem. Eng. J. Adv. 10 (February) (2022), https://doi.org/10.1016/j.ceja.2022.100262, 100262 (1–16).
[37] V. Subramanian, R.K. Roeder, E.E. Wolf, Synthesis and UV-visible-light photoactivity of noble-metal-$SrTiO_3$ composites, 45 (2006) 2187–2193. doi: 10.1021/ie050693y.
[38] M.F. Ordoñez, G. Cerrato, A. Giordana, A. Di Michele, E. Falletta, C.L. Bianchi, One-pot synthesis of Ag-modified $SrTiO_3$: synergistic effect of decoration and doping for highly efficient photocatalytic NOx degradation under LED, J. Environ Chem. Eng. 11 (5) (2023), https://doi.org/10.1016/j.jece.2023.110368, 110368 (1–11).
[39] Q. Zhang, Y. Huang, L. Xu, J.J. Cao, W. Ho, S.C. Lee, Visible-light-active plasmonic Ag-$SrTiO_3$ nanocomposites for the degradation of NO in air with high selectivity, ACS Appl. Mater. Interfaces 8 (6) (2016) 4165–4174, https://doi.org/10.1021/acsami.5b11887.
[40] H. Ma, W. Yang, H. Tang, Y. Pan, W. Li, R. Fang, Y. Shen, F. Dong, Enhance the stability of oxygen vacancies in $SrTiO_3$ via metallic Ag modification for efficient and durable photocatalytic NO abatement, J. Hazard. Mater. 452 (February) (2023), https://doi.org/10.1016/j.jhazmat.2023.131269, 131269(1–10).
[41] M. Stucchi, D. Meroni, G. Safran, A. Villa, C.L. Bianchi, L. Prati, Noble metal promoted TiO_2 from silver-waste valorisation: synergism between Ag and Au, Catalysts 12 (2) (2022) 1–17, https://doi.org/10.3390/catal12020235.
[42] B. Yin, H. Ma, S. Wang, S. Chen, Electrochemical synthesis of silver nanoparticles under protection of poly(N-vinylpyrrolidone), J. Phys. Chem. B 107 (34) (2003) 8898–8904, https://doi.org/10.1021/jp0349031.
[43] T. Standard, "INTERNATIONAL STANDARD Test method for air-purification performance of semiconducting photocatalytic materials—iTeh STANDARD Removal of PREVIEW nitric oxide iTeh STANDARD PREVIEW," vol. 2016, 2016.
[44] E. Padmini, K. Ramachandran, Investigation on versatile behaviour of Cd doped $SrTiO_3$ perovskite structured compounds, Solid State Commun. 302(November 2018) (2019) 113716(1-9). doi: 10.1016/j.ssc.2019.113716.
[45] B.S. Kwak, J.Y. Do, N.K. Park, M. Kang, Surface modification of layered perovskite Sr_2TiO_4 for improved CO_2 photoreduction with H_2O to CH_4, Sci. Rep. 7 (1) (2017) 1–15, https://doi.org/10.1038/s41598-017-16605-w.
[46] A. Vijay, K. Bairagi, S. Vaidya, Relating the structure, properties, and activities of nanostructured $SrTiO_3$ and SrO-($SrTiO_3$)n (n = 1 and 2) for photocatalytic hydrogen evolution, Mater. Adv. 3 (12) (2022) 5055–5063, https://doi.org/10.1039/d2ma00097k.
[47] L. Fang, W. Dong, F. Zheng, M. Shen, Effects of Gd substitution on microstructures and low temperature dielectric relaxation behaviors of $SrTiO_3$ ceramics, J. Appl. Phys. 112 (3) (2012), https://doi.org/10.1063/1.4745876, 034114(1–9).
[48] K.A. Bogle, S.D. Dhole, V.N. Bhoraskar, Silver nanoparticles: synthesis and size control by electron irradiation, Nanotechnology 17 (13) (2006) 3204–3208, https://doi.org/10.1088/0957-4484/17/13/021.
[49] M. Thommes, K. Kaneko, A.V. Neimark, J.P. Olivier, F. Rodriguez-Reinoso, J. Rouquerol, K.S.W. Sing, Physisorption of gases, with special reference to the evaluation of surface area and pore size distribution (IUPAC Technical Report), Pure Appl. Chem. 87 (9–10) (2015) 1051–1069, https://doi.org/10.1515/pac-2014-1117.
[50] D. Barpuzary, Z. Khan, N. Vinothkumar, M. De, M. Qureshi, Hierarchically grown urchinlike CdS@ZnO and CdS@Al_2O_3 heteroarrays for efficient visible-light-driven photocatalytic hydrogen generation, J. Phys. Chem. C 116 (1) (2012) 150–156, https://doi.org/10.1021/jp207452c.
[51] S. Luo, F. Chai, L. Zhang, C. Wang, L. Li, X. Liu, Z. Su, Facile and fast synthesis of urchin-shaped Fe_3O_4@Bi_2S_3 core-shell hierarchical structures and their magnetically recyclable photocatalytic activity, J. Mater. Chem. 22 (11) (2012) 4832–4836, https://doi.org/10.1039/c2jm16476k.
[52] D.C.L. Vasconcelos, V.C. Costa, E.H.M. Nunes, A.C.S. Sabioni, M. Gasparon, W. L. Vasconcelos, Infrared spectroscopy of titania sol-gel coatings on 316L stainless steel, Mater. Sci. Appl. 02 (10) (2011) 1375–1382, https://doi.org/10.4236/msa.2011.210186.
[53] S. Gholamrezaei, M. Salavati-Niasari, An efficient dye sensitized solar cells based on SrTiO3 nanoparticles prepared from a new amine-modified sol-gel route, J. Mol. Liq. 243 (2017) 227–235, https://doi.org/10.1016/j.molliq.2017.08.031.
[54] K. Deng, H. Fan, Z. He, Z. Zhang, D. Chen, La and Cr co-doped $SrTiO_3$ prepared by citric-combustion method for photocatalytic degradation of antibiotics under visible-light, J. Mater. Sci. Mater. Electron. 34 (22) (2023) 1–16, https://doi.org/10.1007/s10854-023-11026-0.
[55] S.M. Mahdi, M.A. Habeeb, Fabrication and tailored structural and dielectric characteristics of ($SrTiO_3$/NiO) nanostructure doped (PEO/PVA) polymeric blend for electronics fields, Phys. Chem. Solid State 23 (4) (2022) 785–792, https://doi.org/10.15330/pcss.23.4.785-792.
[56] A. Vijay, S. Vaidya, Tuning the morphology and exposed facets of $SrTiO_3$ nanostructures for photocatalytic dye degradation and hydrogen evolution, ACS Appl. Nano Mater. 4 (4) (2021) 3406–3415, https://doi.org/10.1021/acsanm.0c03160.
[57] B. Han, L. Wu, J. Li, X. Wang, Q. Peng, N. Wang, X. Li, A nanoreactor based on $SrTiO_3$ coupled TiO_2 nanotubes confined Au nanoparticles for photocatalytic

hydrogen evolution, Int. J. Hydrogen Energy 45 (3) (2020) 1559–1568, https://doi.org/10.1016/j.ijhydene.2019.11.095.
[58] Y. Zhang, C. Liu, Y. Zhou, J. Wang, A. Li, P.F.X. Corvini, Boosting light harvesting and charge separation over hollow double-shelled Ag@$SrTiO_3$-TiO_2 with Z-scheme heterostructure for highly efficient photocatalytic reduction of nitrate to N_2, Chem. Eng. J. 457(November 2022) (2023) 140992(1-12). doi: 10.1016/j.cej.2022.140992.
[59] C.P.P. Wong, C.W. Lai, K.M. Lee, G.T. Pan, C.M. Huang, T.C.K. Yang, J.C. Juan, Enhanced conductivity boosts the cathodic performance of aluminium-doped $SrTiO_3$ in rechargeable alkaline zinc battery, J. Electrochem. Soc. 168 (8) (2021), https://doi.org/10.1149/1945-7111/ac1d01, 080530(1–10).
[60] Z. Wu, Y. Zhang, X. Wang, Z. Zou, Ag@$SrTiO_3$ nanocomposite for super photocatalytic degradation of organic dye and catalytic reduction of 4-nitrophenol, New J. Chem. 41 (13) (2017) 5678–5687, https://doi.org/10.1039/c7nj00522a.
[61] P. Mei, J. Xiao, X. Huang, A. Ishag, Y. Sun, Enhanced photocatalytic reduction of U (VI) on $SrTiO_3$/g-C_3N_4 composites: synergistic interaction, Eur. J. Inorg. Chem. 2022 (7) (2022) 1–9, https://doi.org/10.1002/ejic.202101005.
[62] S. Zhang, W. Xu, All-printed ultra-flexible organic nanowire artificial synapses, J. Mater. Chem. C 8 (32) (2020) 11138–11144, https://doi.org/10.1039/d0tc02172e.
[63] M.G. Galloni, G. Cerrato, A. Giordana, E. Falletta, C.L. Bianchi, Sustainable solar light photodegradation of diclofenac by nano- and micro-sized $SrTiO_3$, Catalysts 12 (8) (2022), https://doi.org/10.3390/catal12080804, 804(1–17).
[64] B. Tan, Y. Ye, Z. Huang, L. Ye, M. Ma, Y. Zhou, Promotion of photocatalytic steam reforming of methane over Ag^0/Ag^+-$SrTiO_3$, Chinese Chem. Lett. 31 (6) (2020) 1530–1534, https://doi.org/10.1016/j.cclet.2019.11.007.
[65] W. Hou, S.B. Cronin, A review of surface plasmon resonance-enhanced photocatalysis, Adv. Funct. Mater. 23 (13) (2013) 1612–1619, https://doi.org/10.1002/adfm.201202148.
[66] J. Singh, Optical Properties of Condensed Matter and Applications – Wiley Series in Materials for Electronic – amp – Optoelectronic Applications, 2006.
[67] F. Ahmed, M.B. Kanoun, C. Awada, C. Jonin, P.F. Brevet, An experimental and theoretical study on the effect of silver nanoparticles concentration on the structural, morphological, optical, and electronic properties of tio2 nanocrystals, Crystals 11 (12) (2021), https://doi.org/10.3390/cryst11121488, 1488(1–14).
[68] A.A. Yousif, K.A. Aadim, N.A. Hamzah, Influence of Ag doping on optical properties of nanocrystalline titanium dioxide prepared by PLD, IOSR J. Appl. Phys. 08 (05) (2016) 50–56, https://doi.org/10.9790/4861-0805025056.
[69] Z. Zheng, B. Huang, X. Qin, X. Zhang, Y. Dai, Facile synthesis of $SrTiO_3$ hollow microspheres built as assembly of nanocubes and their associated photocatalytic activity, J. Colloid Interface Sci. 358 (1) (2011) 68–72, https://doi.org/10.1016/j.jcis.2011.02.032.
[70] X. Li, J. Yu, M. Jaroniec, Hierarchical Porous Photocatalysts 31 (2020).
[71] H. Cheng, J. Wang, Y. Zhao, X. Han, Effect of phase composition, morphology, and specific surface area on the photocatalytic activity of TiO_2 nanomaterials, RSC Adv. 4 (87) (2014) 47031–47038, https://doi.org/10.1039/c4ra05509h.
[72] N. Haghshenas, E. Falletta, G. Cerrato, A. Giordana, C.L. Bianchi, Tuning the visible-light-driven photocatalytic properties of multi-decorated TiO_2 by noble metals towards both propionic acid and NOx degradation, Catal. Commun. 181 (April) (2023), https://doi.org/10.1016/j.catcom.2023.106728, 106728(1–11).
[73] D.N. Bui, J. Mu, L. Wang, S.Z. Kang, X. Li, Preparation of Cu-loaded $SrTiO_3$ nanoparticles and their photocatalytic activity for hydrogen evolution from methanol aqueous solution, Appl. Surf. Sci. 274 (2013) 328–333, https://doi.org/10.1016/j.apsusc.2013.03.054.
[74] M. Siebenhofer, A. Viernstein, M. Morgenbesser, J. Fleig, M. Kubicek, Photoinduced electronic and ionic effects in strontium titanate, Mater. Adv. 2 (23) (2021) 7583–7619, https://doi.org/10.1039/d1ma00906k.
[75] V. Subramanian, R.K. Roeder, E.E. Wolf, Synthesis and UV-visible-light photoactivity of noble-metal-SrTiO 3 composites, Ind. Eng. Chem. Res. 45 (7) (2006) 2187–2193, https://doi.org/10.1021/IE050693Y.